Shallow donor and DX state in Si doped AlN nanowires grown by molecular beam epitaxy

Rémy Vermeersch, Eric Robin, Ana Cros, Gwenolé Jacopin, Bruno Daudin, Julien Pernot

Shallow donor and DX state in Si doped AlN nanowires grown by molecular beam epitaxy

Rémy Vermeersch[1,2], Eric Robin[3], Ana Cros[4], Gwénolé Jacopin[1], Bruno Daudin[2], Julien Pernot[1]

[1] Univ. Grenoble Alpes, Grenoble INP, Institut Néel, CNRS, 38000 Grenoble, France.

[2] Univ. Grenoble Alpes, CEA, IRIG-PHELIQS, NPSC, 17 rue des martyrs, 38000 Grenoble, France.

[3] Univ. Grenoble Alpes, CEA, IRIG-MEM, LEMMA, 17 rue des martyrs, 38000 Grenoble, France.

[4] Materials Science Institute (ICMUV), University of Valencia, ES-46071 Valencia, Spain

Author to whom correspondence should be addressed: remy.vermeersch@neel.cnrs.fr

Keywords: Aluminum nitride, nanowires, molecular beam epitaxy, doping, electrical characterization, current - voltage measurements.

Si doping of AlN nanowires grown by plasma assisted molecular beam epitaxy was investigated with the objective of fabricating efficient AlN based deep ultra-violet light-emitting-diodes. The Si concentration ranged from 10^{16} to 1.8×10^{21} cm^{-3}. Current-voltage measurements performed on nanowire ensembles revealed an ohmic regime at low bias (below 0.1 V) and a space charge limited regime for higher bias. From temperature dependent current-voltage measurements, the presence of Si donors is evidenced in both shallow and deep DX states with ionization energy of 75 meV and 270 meV respectively. The role of Fermi level pinning on NWs sidewalls is discussed in terms of near surface depletion inducing a favorable formation of shallow Si donors.

Deep ultra-violet (DUV) light-emitting-diodes (LEDs) applications in the 200-350 nm wavelength range are manifold, ranging from short range open air communication and lithography to sanitization, sensing, security and more[1]. Until now, mercury lamps have been the main DUV light source despite drawbacks such as a poor lifetime and low efficiency motivating the search for new solid-state solutions, a trend amplified by the planned ban of mercury-containing devices in future[2].

Aluminum gallium nitride (AlGaN) based materials can provide such solutions thanks to their unique assets, specifically their direct and tunable bandgap varying from 3.5 eV (GaN) to 6.2 eV (AlN). Current technologies based on GaN thin films achieve efficient light emission in the 350-400 nm range. However, for increasing AlN molar fraction and decreasing emission wavelength, limitations appear, namely, an inefficient p- and n-type doping related to higher ionization energy of Mg acceptor and Si donor, respectively[3–7], as well as difficult electrical contacts[8,9] and limited light extraction[10–12].

Nanowire (NW) heterostructures are attractive to address some of those issues. Their unique growth mechanism prevents the formation of extended defects. Due to their geometry, the extraction of light can be potentially enhanced beyond the value already reported when using a patterned sapphire substrate[13]. Besides, the incorporation of dopants is proven to be higher in such NW heterostructures due to eased elastic strain relaxation[14–16].

Silicon, which is the most used shallow donor in GaN, turns to be a deep donor in AlGaN with high AlN molar fraction (> 60-80 %)[3]. Particularly, in AlN, the activation energy of Si was found to be around 275 meV[3,4,17–19]. Moreover, as the AlN molar fraction increases, the formation energy of aluminum vacancies V_{Al} decreases. These vacancies act as compensating acceptor

centers with several negatively charged states[20,21] or by being involved with Si or O atoms[22]. These two effects lead to a poor electron density and overall conductivity in AlN, below 1 $S.cm^{-1}$ [4,17,23,24].

In addition, density functional theory-based approach established that common donors in nitrides exhibit a transition between the shallow (*d)* state to a DX^- stable state through lattice relaxation, according to[25–28]

$$2d^0 \leftrightarrow d^+ + DX^-$$

Long known in III-V materials[29–31], this phenomenon is responsible for the increase in ionization energy of Si from ~70 to ~270 meV at around 90 % AlN molar fraction in AlGaN[3,4,32] and the concomitant formation of self-compensation centers. Consistently, photoconductivity experiments performed by Zeisel and coworkers have demonstrated the presence of DX states in Si:AlN layers[33]. Recently, shallow donors in AlN were reported in Si-implanted AlN after annealing at rather low temperature preventing Si atoms to relax to the stable DX state[34,35].

In the present work, we study the electrical transport properties of Si-doped AlN NWs grown by plasma-assisted molecular beam epitaxy (PA-MBE) under different silicon fluxes. Depending on Si concentrations, it is demonstrated that electrical conduction relies on the combination of shallow and deep Si donors, with ionization energies of 75 meV and 270 meV. Because of surface level pinning, numerical simulations highlight the importance of NW diameter and surface passivation to avoid its full depletion, opening a path for future improvements of DUV LEDs based on Si doped AlN NWs for the n-type region.

All studied samples were grown by PA-MBE under nitrogen-rich conditions on n-type Si (111) wafer. They consist of a 350 nm Si-doped GaN stem, followed by a Si-doped AlN section of around 450 nm covered by a 20 nm Si-doped GaN cap. In all samples, Si:GaN sections are

doped with the same Si flux corresponding to ~$2x10^{20}$ Si/cm^3 measured by energy dispersive X-ray spectroscopy (EDX). The silicon cell temperature (T_{Si}) was varied from sample to sample during the AlN section growth, ranging from 750°C up to 1350°C. Table I summarizes the samples and their growth conditions. Morphological study results are presented in Figure 1. The NW height and diameter extracted from SEM images are displayed in Figure 1f, as a function of the Si cell temperature. Following a stable morphology stage for Si effusion cell temperature lower than 1100°C, a transition occurs resulting in the NW widening from 80 nm to 130 nm, associated with a shortening from 810 nm to 720 nm, respectively. At very high Si flux (T_{Si} > 1250°C), the coalescence due to the widening leads to a plateau of the NW diameter. As previously reported for Si- and Mg- doped GaN NWs[16,36,37], this morphology change can be assigned to an enhancement of adatom diffusion on the NW lateral m-planes, leading to a higher incorporation on top of the sidewalls and an increase in radial growth rate compared to the axial one. The formation of a defective shell around the nanowire as identified by Fang et al. for heavily Si-doped GaN NWs[16], with a transition from 6-fold to 12-fold symmetry is not observed. Noticeably, Raman spectroscopy reveals an increase in the full width at half maximum (FWHM) of the E_{2h} peak starting at a T_{Si} ~1200°C, i.e. for a Si flux higher than the flux corresponding to the onset of NW widening (Figure 1f). Then it appears that the increased Al adatom diffusion length on the sidewalls assigned to a Si-induced surfactant effect will impact the NW morphology at a Si flux significantly lower than the flux responsible for the increase in E_{2h} peak FWHM. Interestingly, no shift in the E_{2h} peak energy was observed even for the highest Si flux (Figure S.1). This points towards a non-strained ensemble of NWs in average with large inhomogeneities at the single NW scale without dopant induced strain change. Si content was determined by EDX and corresponding concentrations are reported on table 1 and on the top x-axis of Figure 1. With a detection limit of around $5x10^{18}$ cm^{-3}, only an average Si concentration

from S1200 to S1350 was measured ranging from $6.5x10^{19}$ cm^{-3} to $1.8x10^{21}$ cm^{-3} and extrapolation was done for the rest of the samples (Supplementary 3). EDX results indicate a Si content lower than the solubility limit in AlN, reported to occur for $6x10^{21}$ cm^{-3} in layers [23,38], consistent with the absence of symmetry alteration.

For electrical transport measurements, 100x100 μm^2 Ti/Al pads were deposited as top contact while bottom contact was directly taken on the n-Si substrate. Electrical characterizations were carried out using two probes current-voltage (I-V) measurements. Contact resistances are assumed to be of limited influence on the measurements thanks to highly conductive n-GaN stem and cap with metallic behavior[16], making the GaN contribution negligible with respect to the high resistance of n-AlN section. I-V characteristics presented on a log-log plot in Figure 2.a show a linear regime $I \propto V$ at bias lower than ~0.1 V corresponding to ohmic transport followed by a supralinear regime. This behavior is attributed to a space-charge limited current regime (SCLC) in which electrons are injected from the contact into a material with a low free carrier concentration[39–41] as previously reported in GaN and AlGaN structures[42–45]. SCLC regime occurring at rather low voltages is consistent with an inefficient n-type doping of AlN NWs. Fitting of the linear regime (below 0.1 V) with Ohm's law $I = GV$ gives access to the conductance G, which is reported on a log-scale in Figure 2.b and in table 1. The room temperature conductance versus Si cell temperature describes a bell-like curve for the samples with the lowest Si cell temperatures (T_{Si} below 1200°C) where the maximum of conductance reaches a value of $1.4x10^{-5}$ S for S900 at [Si] ~ $6x10^{16}$ cm^{-3}. This behavior is expected from the self-compensation of Si already observed by Harris et al.[22] in the same range of concentration in case of thin films. The conductance for the samples with the highest Si cell temperatures (T_{Si} above 1200°C) shifts toward higher values. This increase is assigned to the increase in NW

diameter which reduces the impact of the surface on wire depletion. This point will be detailed later. Due to its morphology, electrical characterization of S1350 will not be discussed.

Temperature dependent I-V measurements were performed in order to probe the ionization properties of the Si donors in AlN NWs. Figures 3.a and 3.b show typical I-V curves for samples S900 and S1300 at different temperatures. For each temperature, the conductance was extracted from a fit of the linear regime and plotted as a function of 1000/T in Figure 3.c - 3.d. For samples with $T_{Si} < 1200°C$ (Figure 3.c), two regimes are present in all measured samples and fitting with $G = G_1 \exp\left(-\frac{E_{D1}}{kT}\right) + G_2 \exp\left(-\frac{E_{D2}}{kT}\right)$ was used to extract conductance values and activation energies of the different regimes. Values of the fitting parameters are reported in table 1. At lower temperatures, an ionization energy of 75 meV is extracted which is consistent with the shallow donor state of Si in AlN[34,35] and predicted by the hydrogenic model. At higher temperature, an ionization energy of 270 meV is found, which is attributed to the DX state of Si[33,34,46–48]. Interestingly, S0 and S800 exhibit a higher activation energy of around 700 meV at high temperature, which is inferred from the ionization energy of residual oxygen in DX state in AlGaN[49]. The energy of 75 meV found in the lower temperature range for these samples probably arises from the hydrogenic state of residual O, indistinguishable from the Si one[27,50,51]. Regarding samples grown with $T_{Si} \geq 1200°C$, (Figure 3.d) the signature of the DX state is predominant. As shown on figure 3.e, persistent photocurrent (PPC) was observed in S1200 whereas absent in S900, under a 500 nm illumination. Below bandgap illumination does not generate electron-hole pairs which discard the effect of charge splitting induced by Fermi level pinning, as reported in Calarco et al. in the case of GaN NWs[44]. It rather indicates that the deep donor behaves like an electron trap when the light is turned off, which could be due to optical excitation of DX center[30,33,48,52] (Supplementary 4).

The presence of both shallow and deep Si donors can have multiple origins. DX state formation is directly linked to thermodynamic equilibrium in which a Si atom lowers its energy through lattice relaxation. Being out of equilibrium is the reason claimed by Breckenridge and coworkers for the presence of shallow donors in implanted Si:AlN[34]. Due to NW dimensions, surface level pinning arising from surface states at the side walls significantly modifies the near-surface energy band diagram. A Fermi level pinning on m-plane AlN at 2.1 eV below CB was reported[53]. In the work of Gordon et al. formation energy diagram of *d* and DX^- states was computed and showed a transition between the two occurring at 150 meV and 640 meV below CB for Si and O respectively[27]. Because of the large pinning, effective Fermi level in NWs is expected to lay below these values, for which Si incorporation in *d* state is favored. This hypothesis matches the experimental data where shallow donors are found to be the main contributors for the smallest diameter where the influence of Fermi level pinning is higher. For wider NWs, growth occurs closer to the bulk case in which DX states formation is more favorable.

As seen in Figure 2.b, an increase of 2 orders of magnitude in the conductance occurs for a T_{Si} between 1100°C and 1200°C. This sudden increase is opposite to the observed trend and to the higher ionization energy found previously. It is assumed to result from the increased diameter from ~80 nm to ~130 nm for the highest Si cell temperatures. Indeed, the small diameter of AlN NWs makes them particularly sensitive to surface states and Fermi level pinning. In the case of non-intentionally doped GaN NWs, Calarco et al. found a Fermi level pinned around 0.55 eV below conduction band (CB) on m-planes[44]. The complete depletion of GaN NWs doped with a Si concentration of 1.8×10^{18} cm^{-3} was reached for a NW diameter of 50 nm. In the present case, the large value of 2.1 eV is consistent with a full depletion of the AlN NWs especially for the lowest Si flux. This hypothesis is further supported by the improved electrical conduction

properties after heating under vacuum or exposed to electron beam, which is assigned to desorption of species changing the surface charge state (Supplementary 5).

To quantitatively investigate the depletion and surface effect on AlN NWs properties, NextNano^{++}[54] simulations were performed in order to solve neutrality equation in the studied system. Results are displayed in Figure 4. An ionization energy of 75 meV and no compensation were assumed. Figure 4.a displays the CB minimum in the NW plane with a Fermi level pinning at 2.1 eV from the CB whereas Figure 4.b displays the local electron density for 10^{19} donors/cm^3. In this case, it appears that the NW is not fully depleted but electrons are located in the center of the wire. In order to evaluate the depletion region width, we compared the calculated electron densities n in the case of the NWs with the value n_{FB} obtained for bulk (i.e. with flat band at surfaces) and plotted the ratio of the two: Figure 4.c shows a cross section of the NWs with band-edges in blue for a donor concentration of 10^{19} cm^{-3}, in addition to the ratio n/n_{FB} versus the position for three donor concentrations. For a diameter of 80 nm and $N_D < 2x10^{18}$ cm^{-3} the wire is fully depleted whereas for $N_D = 3x10^{18}$ cm^{-3} only the core is expected to have an electron density equal to 70% of the bulk one. Full or partial depletion of the wire results in drastic reduction of the free carrier density and consequently in conductance. An effective free electron density in the NW n_{eff} is defined as the average electron density in the nanowire, following equation (1):

$$n_{eff} = \frac{1}{S}\int_S n(x,y)dxdy \quad (1)$$

As shown in figure 4.d, the NW width increase from 80 nm to 130 nm leads to an increase of several orders of magnitude in the effective carrier density in the 10^{18} N_D/cm^3 range, the smaller wires being fully depleted while the larger are not. Moreover, the effect is similar if instead of widening the wire, the Fermi level pinning is lowered to 1 eV (Supplementary 6). This demonstrates the relevance of surface passivation in AlN NWs to enhance conduction properties.

In this figure values from the literature are also reported, highlighting the increase of more than one order of magnitude in free carrier concentration by changing the ionization energy from 270 meV to 75 meV. Since all samples are conductive at room temperature none of them were fully depleted, which seems to indicate a lower Fermi level pinning or the presence of residual O donors in the low Si doped and undoped samples (Figure 3.a) with donor density N_D = [Si] + [O] larger than $2x10^{18}$ cm^{-3}. Because of the small dimensions, shallow donors are in larger quantities and can contribute to the conduction while the deep donors in minority are frozen (S0 - S900). At higher Si concentration, the number of compensating states increases and leads to the reduction of conductance (S900 - S1100). As Si flux becomes larger and the wires widen, DX incorporation is favored and conduction occurs thanks to deep DX states with a continuous increased compensation (S1200 - S1300).

To summarize, we have studied the Si doping of AlN NWs grown by MBE. A change in growth mechanism occurs above an effusion cell temperature of 1100 °C and a Si concentration of about $9x10^{18}$ Si/cm^{-3}. Through NW morphology studies we assessed Si concentration lower than solubility limit and a preserved strain state. I-V characteristics were performed by two-probe measurements and showed the presence of both ohmic and SCLC regime, which indicates a low number of free carriers at equilibrium attributed to partial depletion of the wire. The presence of both shallow and deep Si donors was assessed by temperature dependent I-V measurements. Shallow donor incorporation has been tentatively assigned to a Fermi level far from stability domain of DX centers during the growth. We also showed that the NW diameter is of critical influence as well as Fermi level pinning which can both be particularly detrimental in terms of electrical properties. For this purpose, effect of surface passivation should be studied as it could be of particular interest to improve the conductivity.

Supplementary material:

See supplementary materials for experimental details as well as additional experiments mentioned in the text.

Acknowledgements:

The authors thank Y. Genuist, Y. Curé and F. Jourdan from CEA Grenoble for technical support during MBE growth, F. Donatini for the realization of the persistent photocurrent experimental setup and the Nanofab team from Néel Institute for the use of their facilities and technical assistance. A. Cros acknowledges financial support from Project PROMETEO/2018/123 from Generalitat Valenciana and SCSIE for technical support during Raman measurements.

Data Availability

The data that support the findings of this study are available from the corresponding author upon reasonable request.

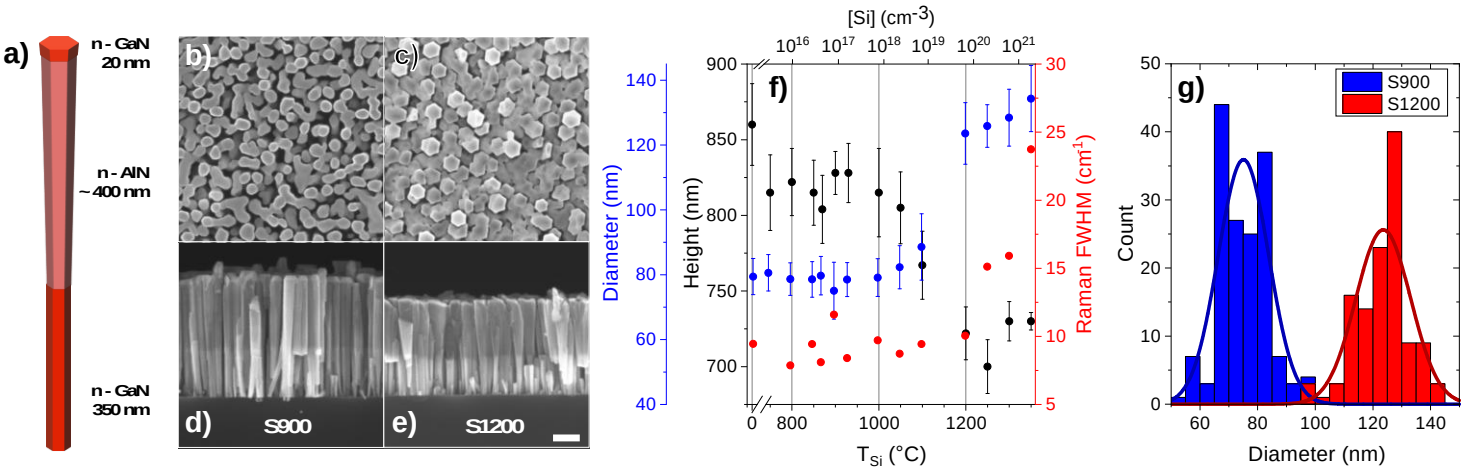

FIG. 1: (a) Schematic of the NW structure under investigation. (b, c) Top view and (d, e) cross section SEM images of S900 (b, d) and S1200 (c, e). The scale bar of 200 nm is the same for all SEM images. (f) NW diameter (blue), height (black) and Raman full width at half maximum (red) as a function of Si cell temperature and Si concentration. Dots represent data points with their error bar while full lines are guide for the eye. (g) NW diameter histograms for S900 (blue) and S1200 (red). Lines are fits with gaussian distribution.

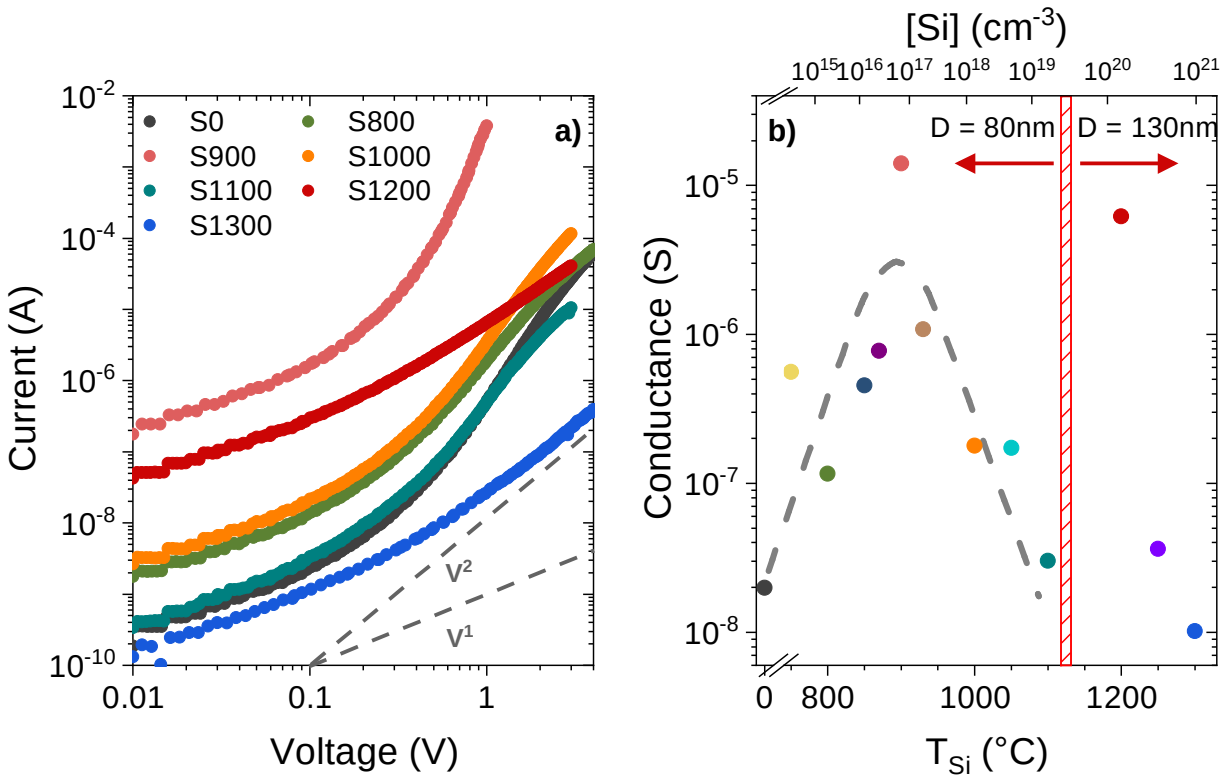

FIG. 2: (a) Room temperature I-V characteristics of samples obtained from two probes experiments. The black vertical dashed line represents the transition between ohmic and space-charge limited current behavior. (b) Conductance extracted from the low voltage ohmic regime as function of the Si cell temperature for all samples under study. The dotted line is a guide for the eyes and the red crosshatched rectangle materializes the morphology transition boundary.

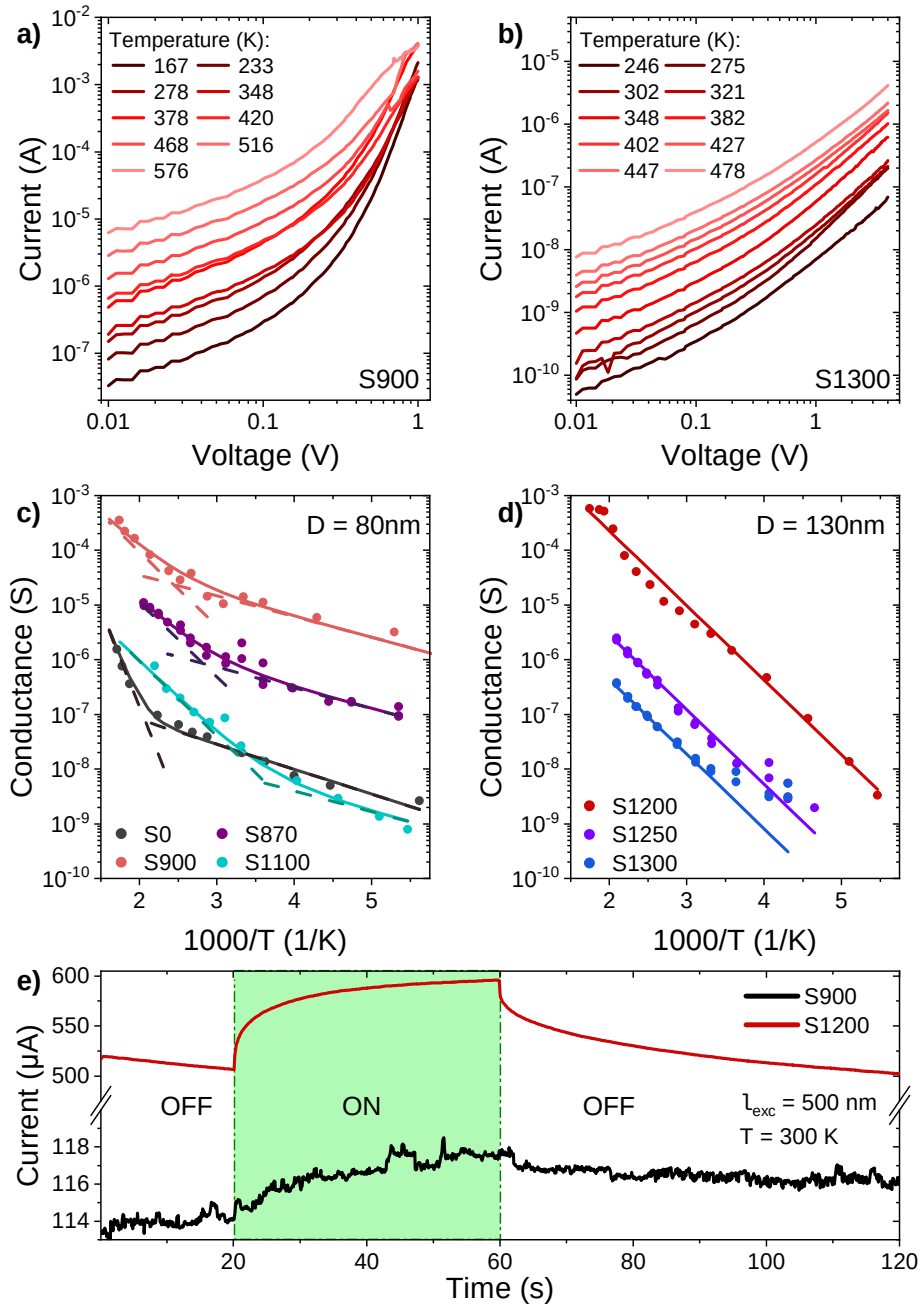

FIG. 3: (a, b) I-V characteristics for different temperatures for samples S900 (a) and S1300 (b). (c, d) Arrhenius plot of the conductance extracted from ohmic regime for the samples with a diameter of 80nm (c) and 130nm (d). (e) Current at +1 V over time for S900 and S1200 at room temperature with or without illumination under a 500 nm light.

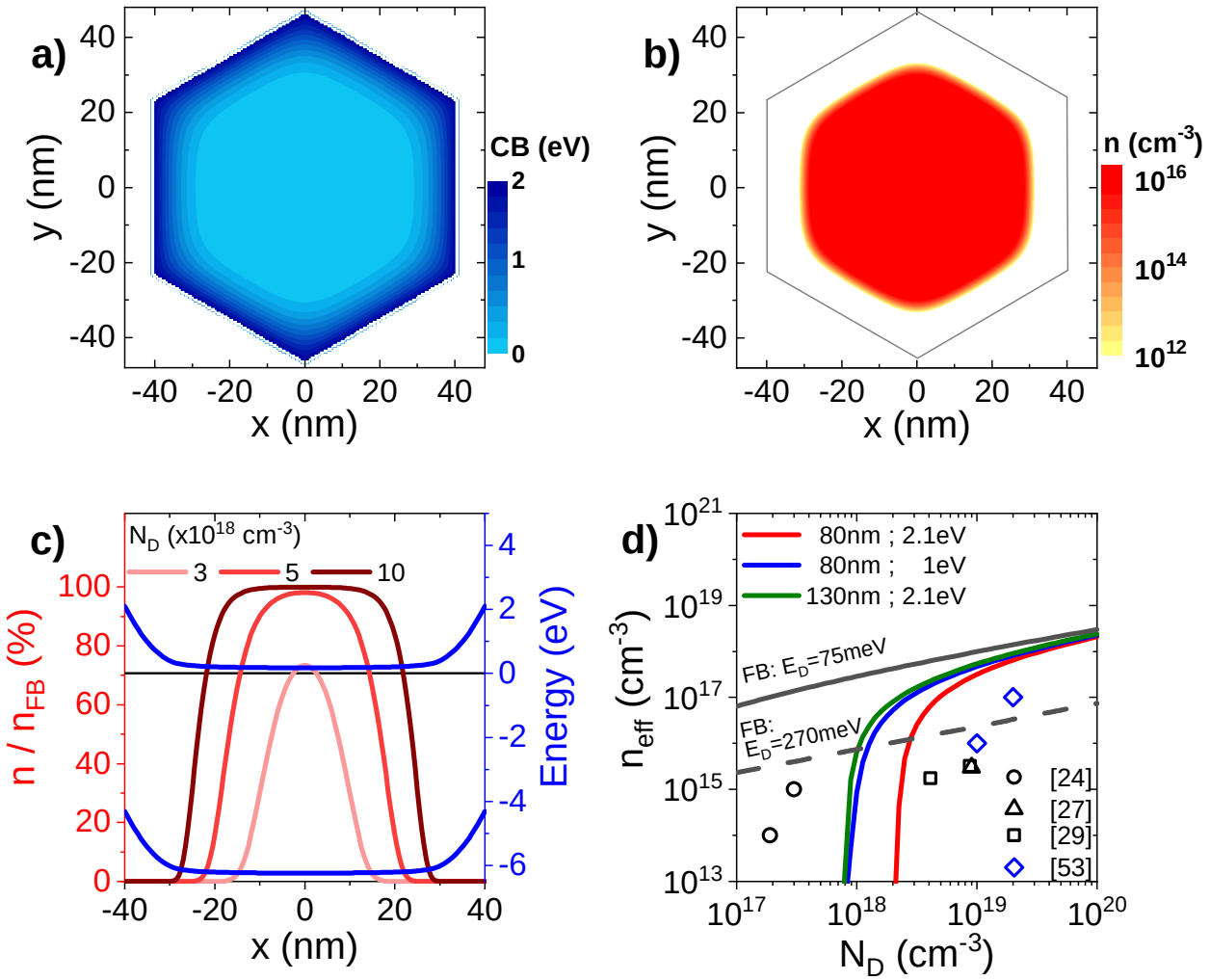

FIG. 4: (a) Simulated conduction band minimum and (b) electron density in the NW plane. (c) Ratio between NW and bulk electron density (red) and conduction and valence bands (blue) as a function of the position in the NW. Fermi level is represented by the black line at 0 eV. All simulations have been computed with NextNano^{++} [54] for a Fermi level pinning of 2.1 eV on m-plane, a donor concentration of 10^{19} cm^{-3} and a donor ionization energy of 75 meV. Only n/n_{FB} ratio simulations were performed for donor concentration varying from 3x10^{18} cm^{-3} to 1x10^{19} cm^{-3}, as indicated in the figure. (d) Simulated effective electron density for two different NW diameters and Fermi level pinning as a function of the donor concentration. Black and blue markers are reported values with an ionization energy of 270 meV and 86 meV respectively.

TABLE I. Description of studied samples with their structural parameters, conductance at room temperature G_{300K} and ionization energies $E_{D1,2}$ used for the fits. A unique value for E_{D1} and E_{D2} have been used to fit the whole set of samples. [Si] data marked with * means interpolated values (Supplementary 3).

Sample name	T_{Si} (°C)	[Si] (cm^{-3})	NW diameter (nm)	NW length (nm)	G_{300K} (S)	E_{D1} (meV)	E_{D2} (meV)
S0	No Si		79	860	$2.0x10^{-8}$	75	700
S750	750	$2.4x10^{15}$ *	81	815	$5.6x10^{-7}$	Not measured	
S800	800	$1.7x10^{15}$ *	79	822	$1.2x10^{-7}$	75	700
S850	850	$1.0x10^{16}$ *	79	815	$4.6x10^{-7}$	Not measured	
S870	870	$2.2x10^{16}$ *	80	804	$7.8x10^{-7}$	75	270
S900	900	$5.2x10^{16}$ *	75	828	$1.4x10^{-5}$	75	270
S930	930	$1.3x10^{17}$ *	79	828	$1.1x10^{-6}$	Not measured	
S1000	1000	$9.5x10^{17}$ *	79	815	$1.8x10^{-7}$	75	270
S1050	1050	$3.4x10^{18}$ *	82	805	$1.7x10^{-7}$	75	270
S1100	1100	$9.4x10^{18}$ *	89	767	$3.1x10^{-8}$	75	270
S1200	1200	$6.5x10^{19}$	125	722	$6.2x10^{-6}$	Not observed	270
S1250	1250	$2.0x10^{20}$	126	700	$3.6x10^{-8}$	Not observed	270
S1300	1300	$6.0x10^{20}$	128	730	$1.0x10^{-8}$	Not observed	270

References

[1] M. Kneissl, T.-Y. Seong, J. Han, and H. Amano, Nat. Photonics **13**, 233 (2019).

[2] United Nations, (2017).

[3] P. Pampili and P.J. Parbrook, Mater. Sci. Semicond. Process. **62**, 180 (2017).

[4] M.L. Nakarmi, K.H. Kim, K. Zhu, J.Y. Lin, and H.X. Jiang, Appl. Phys. Lett. **85**, 3769 (2004).

[5] F. Mireles and S.E. Ulloa, Mater. Res. Soc. Symp. - Proc. **482**, 839 (1997).

[6] Y. Taniyasu, M. Kasu, and T. Makimoto, Nature **441**, 325 (2006).

[7] F. Mehnke, X.T. Trinh, H. Pingel, T. Wernicke, E. Janzén, N.T. Son, and M. Kneissl, J. Appl. Phys. **120**, 1 (2016).

[8] T. Mori, T. Kozawa, T. Ohwaki, Y. Taga, S. Nagai, S. Yamasaki, S. Asami, N. Shibata, and M. Koike, Appl. Phys. Lett. **69**, 3537 (1996).

[9] R. France, T. Xu, P. Chen, R. Chandrasekaran, and T.D. Moustakas, Appl. Phys. Lett. **90**, 3 (2007).

[10] T. Takano, T. Mino, J. Sakai, N. Noguchi, K. Tsubaki, and H. Hirayama, Appl. Phys. Express **10**, (2017).

[11] B.K. Saifaddin, A. Almogbel, C.J. Zollner, H. Foronda, A. Alyamani, A. Albadri, M. Iza, S. Nakamura, S.P. Denbaars, and J.S. Speck, Semicond. Sci. Technol. **34**, 035007 (2019).

[12] C. Reich, M. Guttmann, M. Feneberg, T. Wernicke, F. Mehnke, C. Kuhn, J. Rass, M.

Lapeyrade, S. Einfeldt, A. Knauer, V. Kueller, M. Weyers, R. Goldhahn, and M. Kneissl, Appl. Phys. Lett. **107**, 1 (2015).

[13] H. Hu, B. Tang, H. Wan, H. Sun, S. Zhou, J. Dai, C. Chen, S. Liu, and L.J. Guo, Nano Energy **69**, 104427 (2020).

[14] A.-M. Siladie, G. Jacopin, A. Cros, N. Garro, E. Robin, D. Caliste, P. Pochet, F. Donatini, J. Pernot, and B. Daudin, Nano Lett. **19**, 8357 (2019).

[15] Y.B. Tang, X.H. Bo, J. Xu, Y.L. Cao, Z.H. Chen, H.S. Song, C.P. Liu, T.F. Hung, W.J. Zhang, H.M. Cheng, I. Bello, S.T. Lee, and C.S. Lee, ACS Nano **5**, 3591 (2011).

[16] Z. Fang, E. Robin, E. Rozas-Jiménez, A. Cros, F. Donatini, N. Mollard, J. Pernot, and B. Daudin, Nano Lett. **15**, 6794 (2015).

[17] Y. Taniyasu, M. Kasu, and T. Makimoto, Appl. Phys. Lett. **85**, 4672 (2004).

[18] R. Collazo, S. Mita, J. Xie, A. Rice, J. Tweedie, R. Dalmau, and Z. Sitar, Phys. Status Solidi **8**, 2031 (2011).

[19] Y. Taniyasu, M. Kasu, and T. Makimoto, Appl. Phys. Lett. **89**, 9 (2006).

[20] T. Mattila and R. Nieminen, Phys. Rev. B - Condens. Matter Mater. Phys. **55**, 9571 (1997).

[21] C.G. Van De Walle and J. Neugebauer, J. Appl. Phys. **95**, 3851 (2004).

[22] J.S. Harris, J.N. Baker, B.E. Gaddy, I. Bryan, Z. Bryan, K.J. Mirrielees, P. Reddy, R. Collazo, Z. Sitar, and D.L. Irving, Appl. Phys. Lett. **112**, (2018).

[23] M. Hermann, F. Furtmayr, A. Bergmaier, G. Dollinger, M. Stutzmann, and M. Eickhoff, Appl. Phys. Lett. **86**, 1 (2005).

[24] F. Mehnke, T. Wernicke, H. Pingel, C. Kuhn, C. Reich, V. Kueller, A. Knauer, M. Lapeyrade, M. Weyers, and M. Kneissl, Appl. Phys. Lett. **103**, 9 (2013).

[25] P. Bogusławski and J. Bernholc, Phys. Rev. B **56**, 9496 (1997).

[26] C. Park and D. Chadi, Phys. Rev. B - Condens. Matter Mater. Phys. **55**, 12995 (1997).

[27] L. Gordon, J.L. Lyons, A. Janotti, and C.G. Van De Walle, Phys. Rev. B - Condens. Matter Mater. Phys. **89**, 1 (2014).

[28] C.G. Van de Walle, Phys. Rev. B - Condens. Matter Mater. Phys. **57**, R2033 (1998).

[29] D.J. Chadi and K.J. Chang, Phys. Rev. Lett. **61**, 873 (1988).

[30] P.M. Mooney, J. Appl. Phys. **67**, R1 (1990).

[31] M.G. Craford, G.E. Stillman, J.A. Rossi, and N. Holonyak, Phys. Rev. **168**, 867 (1968).

[32] B. Borisov, V. Kuryatkov, Y. Kudryavtsev, R. Asomoza, S. Nikishin, D.Y. Song, M. Holtz, and H. Temkin, Appl. Phys. Lett. **87**, 1 (2005).

[33] R. Zeisel, M. Bayerl, S. Goennenwein, R. Dimitrov, O. Ambacher, M. Brandt, and M. Stutzmann, Phys. Rev. B - Condens. Matter Mater. Phys. **61**, R16283 (2000).

[34] M. Hayden Breckenridge, Q. Guo, A. Klump, B. Sarkar, Y. Guan, J. Tweedie, R. Kirste, S. Mita, P. Reddy, R. Collazo, and Z. Sitar, Appl. Phys. Lett. **116**, 172103 (2020).

[35] M.H. Breckenridge, P. Bagheri, Q. Guo, B. Sarkar, D. Khachariya, S. Pavlidis, J. Tweedie, R. Kirste, S. Mita, P. Reddy, R. Collazo, and Z. Sitar, Appl. Phys. Lett. **118**, (2021).

[36] F. Furtmayr, M. Vielemeyer, M. Stutzmann, J. Arbiol, S. Estrad́, F. Peir, J.R. Morante, and M.

Eickhoff, J. Appl. Phys. **104**, (2008).

[37] A.-M. Siladie, L. Amichi, N. Mollard, I. Mouton, B. Bonef, C. Bougerol, A. Grenier, E. Robin, P.-H. Jouneau, N. Garro, A. Cros, and B. Daudin, Nanotechnology **29**, 255706 (2018).

[38] M. Kasu, Y. Taniyasu, and N. Kobayashi, Jpn. J. Appl. Phys. **40**, L1048 (2001).

[39] N.F. Mott and R.W. Gurney, *Electronic Processes in Ionic Crystals* (1940).

[40] A. Rose, Phys. Rev. **97**, 1538 (1955).

[41] M.A. Lampert, Phys. Rev. **103**, 1648 (1956).

[42] A.A. Talin, B.S. Swartzentruber, F. Léonard, X. Wang, and S.D. Hersee, J. Vac. Sci. Technol. B Microelectron. Nanom. Struct. **27**, 2040 (2009).

[43] V. Lebedev, G. Cherkashinin, G. Ecke, I. Cimalla, and O. Ambacher, J. Appl. Phys. **101**, (2007).

[44] R. Calarco, T. Stoica, O. Brandt, and L. Geelhaar, J. Mater. Res. **26**, 2157 (2011).

[45] Z. Fang, F. Donatini, B. Daudin, and J. Pernot, Nanotechnology **29**, 01LT01 (2018).

[46] S.T.B. Goennenwein, R. Zeisel, O. Ambacher, M.S. Brandt, M. Stutzmann, and S. Baldovino, Appl. Phys. Lett. **79**, 2396 (2001).

[47] K. Thonke, M. Lamprecht, R. Collazo, and Z. Sitar, Phys. Status Solidi Appl. Mater. Sci. **214**, (2017).

[48] X.T. Trinh, D. Nilsson, I.G. Ivanov, E. Janzén, A. Kakanakova-Georgieva, and N.T. Son, Appl. Phys. Lett. **105**, (2014).

[49] M.D. McCluskey, N.M. Johnson, C.G. Van de Walle, D.P. Bour, M. Kneissl, and W. Walukiewicz, Phys. Rev. Lett. **80**, 4008 (1998).

[50] Y. Taniyasu, M. Kasu, and N. Kobayashi, Appl. Phys. Lett. **81**, 1255 (2002).

[51] T. Mattila and R. Nieminen, Phys. Rev. B - Condens. Matter Mater. Phys. **54**, 16676 (1996).

[52] D. V. Lang, R.A. Logan, and M. Jaros, Phys. Rev. B **19**, 1015 (1979).

[53] P. Reddy, I. Bryan, Z. Bryan, W. Guo, L. Hussey, R. Collazo, and Z. Sitar, J. Appl. Phys. **116**, (2014).

[54] S. Birner, (n.d.).